Excited state intramolecular proton transfer (ESIPT) in 2-(2 '-hydroxyphenyl)benzoxazole and its naphthalene-fused analogs: A TD-DFT quantum chemical study

ARTICLE *in* SPECTROCHIMICA ACTA PART A MOLECULAR AND BIOMOLECULAR SPECTROSCOPY · AUGUST 2013

Impact Factor: 2.35 · DOI: 10.1016/j.saa.2013.08.068 · Source: PubMed

4 AUTHORS, INCLUDING:

Hossein Roohi
University of Guilan
74 PUBLICATIONS **423** CITATIONS
SEE PROFILE

Mahjoubeh Jahantab
University of Guilan
7 PUBLICATIONS **24** CITATIONS
SEE PROFILE

Spectrochimica Acta Part A: Molecular and Biomolecular Spectroscopy 118 (2014) 228–238

Contents lists available at ScienceDirect

Spectrochimica Acta Part A: Molecular and Biomolecular Spectroscopy

journal homepage: www.elsevier.com/locate/saa

Excited state intramolecular proton transfer (ESIPT) in 2-(2′-hydroxyphenyl)benzoxazole and its naphthalene-fused analogs: A TD-DFT quantum chemical study

Hossein Roohi *, Fahimeh Hejazi, Nafiseh Mohtamedifar, Mahjobeh Jahantab

Department of Chemistry, Faculty of Science, University of Guilan, P.O. Box 98135-674, Rasht, Iran

HIGHLIGHTS

- DFT/TDDFT method has been performed to study the ESIPT.
- Estimation of strength of H-bonding interactions in HBO and HNB1–3.
- Low energy barrier in excited state.
- Relationship between the position of π conjugation system and the occurrence of ESIPT reaction.
- Agreement between theoretical and experimental absorption and emission bands.

GRAPHICAL ABSTRACT

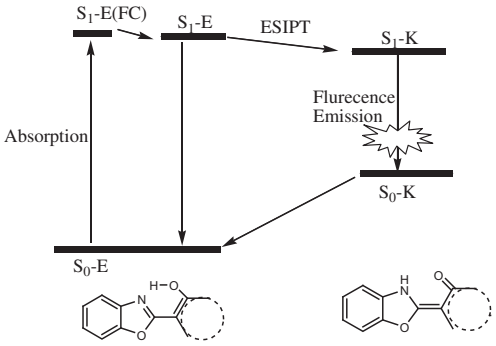

ARTICLE INFO

Article history:
Received 10 July 2013
Received in revised form 12 August 2013
Accepted 15 August 2013
Available online 29 August 2013

Keywords:
ESIPT
H-bonding
Excitation energy
PBE1PBE
AIM

ABSTRACT

The intramolecular proton transfer reactions in 2-(2′-hydroxyphenyl)benzoxazole (**HBO**) and its naphthalene-fused analogs, (**HNB1–3**) in both S_0 and S_1 states at the PBE1PBE/6-311++G(2d,2p) level of theory in the gas phase and water have been investigated to find the effects of extension of aromaticity on the intramolecular proton transfer and photophysical properties. The results show that the ground state intramolecular proton transfer (GSIPT) in the studied species is impossible. Excited states potential energy surface calculations support the existence of ESIPT process. Structural parameters, relative energy of isomers, H-bonding energy, adsorption and emission bands, vertical excitation and emission energies, oscillator strength, fluorescence rate constant, dipole moment, atomic charges and electron density at critical points were calculated. Orbital analysis shows that vertical $S_0 \rightarrow S_1$ transition in the studied molecules corresponds essentially to the excitation from HOMO (π) to LUMO (π*). The potential of **HNB2** molecule as an emissive and electron transport material in designing improved organic white light emitting diodes is predicted in this work. Our calculations are also supported by the experimental observations.

Introduction

Excited-state intramolecular proton transfer (ESIPT) is a photo-induced procedure in which a proton jumps across the intramolecular hydrogen bond (IMHB) from a proton donor group to a proton acceptor one which first described by Waller [1]. In recent years, there has been an increasing attention in ESIPT [2–12] because of its wide applications to such systems as UV-light polymer stabilizers, laser dyes, molecular switches fluorescence sensors, and particularly in biological systems [13–21]. For instance, it is well accepted that the fluorescence ability of the green fluorescent proteins is controlled by the multiple-proton transfer after photoexcitation [22].

* Corresponding author. Tel.: +98 1313243630x35; fax: +98 1313220066.
E-mail address: hroohi@guilan.ac.ir (H. Roohi).

1386-1425/$ - see front matter © 2013 Elsevier B.V. All rights reserved.
http://dx.doi.org/10.1016/j.saa.2013.08.068

Photoisomerization in the IMHB site in aromatic systems has gained particular attention because of its necessary role in the functionality of so-called photostabillizers which are in wide technical use for the protection of organic polymers against degradation by the UV components of sunlight [23]. Several computational papers published in recent years [24–35] have allowed a remarkable advance toward a full understanding of the photoisomerization process, providing the ground for interpreting the quickly growing amount of experimental results [36–38].

In ESIPT mechanism, there are a number of questions that cannot be answered exclusively by experimental means and that call for a detailed theoretical investigation. For example, what is the structure of the S_1/S_0 systems? Why the ESIPT processes occur? What is the origin of ESIPT mechanism? Computational quantum chemistry study on relevant model systems is a promising way to reveal the mechanism of the proton transfer through the IMHB process. Recent researches on ESIPT process have addressed quinoline [33,39] and benzylidine [35] derivatives. They have shown that the enol form is stable in the ground state, and conversion from the enol to the keto form occurs very rapidly after excitation.

The 2-(2′-hydroxyaryl)benzoxazole (**HBO**) may be a quit interesting compound which exhibits phototautomerization. Photochemistry of parent compound of our study, **HBO**, has been widely investigated experimentally and theoretically [40–44]. The experimental results have been revealed that the excited state proton transfer in **HBO** can be affected by degree of π-conjugation [41]. Moreover, ESIPT is strongly influenced by the nature of the substituents and their attachment positions [45], resulting in the shift of absorption and emission peaks. Recently, a small Stokes-shifted fluorescence from the excited state keto form of a naphthalene-fused analog of **HBO**, 2-(2′-Hydroxynaphthyl) benzoxazole, has been reported [41]. The Stokes shift is a measure of the structural change that occurs upon excitation from the ground state stable form to the excited state stable form. The different isomers of 2-(2′-Hydroxynaphthyl) benzazole (**HNB1–3)** can be created by change in the position of benzene ring linked to the phenol ring. In recent years, we have studied ground state proton transfer reactions in different systems [46]. To the best of our knowledge, there are no computational and experimental studies that in detailed address the effect of expansion and position of aromatic ring on the ESIPT process in **HBO** and **HNB1–3**. In this work, we have investigated the effect of π-conjogation on the photophysics and photochemistry of these molecules with particular emphasis on the nature and mechanism of the ESIPT reaction. In addition, H-bonding interaction along the proton transfer between enol– and keto–froms of the **HBO** and **HNB1–3** are characterized by quantum theory of atoms in molecules (QTAIM) [47–49] analyses.

Computational details

The stationary points on the S_0 and S_1 potential energy surfaces of **HBO** and **HNB1–3** were optimized using DFT methods (PBE1PBE for S_0) and (PBE1PBE-TD for S_1) [50] in conjunction with the 6-311++G(2d,2p) basis set. DFT methods are used as a reliable standard tool for the theoretical treatment of electronic structure and spectroscopic properties of various types of compounds. Despite the absence of adjustable parameters, PBE1PBE (TD-PBE1PBE) has already provided excitation spectra in very good agreement with the available experimental results [51,30,32]. Vibration frequency calculations were performed analytically and numerically for the S_0 and S_1 states to obtain vibrational zero point and thermal energies and to validate that the found structures corresponded to the energy-minima or transition states. They confirmed the presence of minima by the absence of imaginary modes and transition states by a single imaginary mode. The calculations were carried out using the GAUUSIAN 03 program package [52]. Bulk solvent effects on the ground and the excited states have been taken into account by means of the polarizable continuum model (PCM) [53]. In this model, the molecule is embedded in a cavity surrounded by an infinite dielectric, with the dielectric constant of the solvent. The Bader theory was also applied to find critical points and to characterize them. The charge on the atoms was calculated by using CHelpG population analysis [54]. Topological properties of bond critical points (BCPs) were calculated at the PBE1PBE/6-311++G(2d,2p) level of theory by using the AIM2000 program package [55].

Results and discussions

The equilibrium structures of the stationary points and their changes provided us with the basis to understand how the molecular structure transformed upon photoexcitation and ESIPT. The optimized structures of **HBO** and **HNB1–3** at the S_0 and S_1 states are given in Fig. 1. The parent compound of our study, **HBO**, is planar with C_s symmetry. The naphthalene-fused analogs of **HBO**, **HNB1–3** molecules are isomers differing only by the position of phenyl group with respect to the OH of phenol ring and bond connecting the two sides of the molecules. Each of the **HBO** and **HNB1–3** molecules can be existed as enole (denoted S_0–E) and keto tautomeric forms (denoted S_0–K). In the S_1 state, two E and K forms are symbolized as S_1–E and S_1–K, respectively. Both forms of the **HNB1–3** are also planar with C_s symmetry.

Fig. 2 illustrates the energy diagram of phototautomerization in the **HBO** and **HNB1–3**. Initially, molecules are in ground state S_0–E. Upon photoexcitation, molecule is vertically excited to Franck–Condon (FC) point with the geometry of the S_0–E state and with the energy difference corresponding to the most intensive peak in the absorption spectrum. The PT reaction starts from the FC point; it passes through the S_1–E state with geometric rearrangement from the FC point by gaining a certain amount of kinetic energy. From S_1–E state, the molecule can undergoes a tautumerization via ESIPT to the excited state S_1–K or emit a photon and return to the S_0–E state. From the S_1–K, molecule emits a photon and fall to the ground state S_0–K with the energy difference corresponding to the fluorescence spectrum. Finally, S_0–K in ground state is relaxed to the S_0–E.

Relative energy of HNB1–3 isomers

The relative energies of **HNB1–3** and H-bond energies are given in Table 1. From these energies, it is obvious that the stability of the S_0–E form of **HNB1–3** in the gas phase decreases in the following order: **HNB1** > **HNB2** > **HNB3**. Thus, **HNB1** and **HNB3** isomers are the most and least stable ones. The value of H-Bond angle in **HNB1–3** is almost 147.5°. In all of the **HNB1–3** isomers, O–H bond is involved in hydrogen bonds with differing strengths, which leads to slightly different intramolecular distance. The selected optimized structural parameters involved in GSIPT and ESIPT reactions are summarized in Table 2. The O–H bond length in the **HBO** and **HNB1–3** isomers is 0.985 and 0.989 Å, 0.982 and 0.996 Å and the N···HO distance is 1.749 and 1.719 Å, 1.759 and 1.626 Å, respectively. Thus, it is predicted that the strength of H-bonding interaction increases on going from **HBO** to **HNB1** and **HNB3** and decrease to **HNB2**. Despite the greater stability of the **HNB1**, H-bonding interaction in **HNB3** is stronger than others. There is a reverse correlation between amount of delocalization of π-electron and the strength of H-bonding pictured by O–H interatomic distance. The longer the O–H interatomic distance is, the more negative charge at the oxygen atom appears and thus the stron-

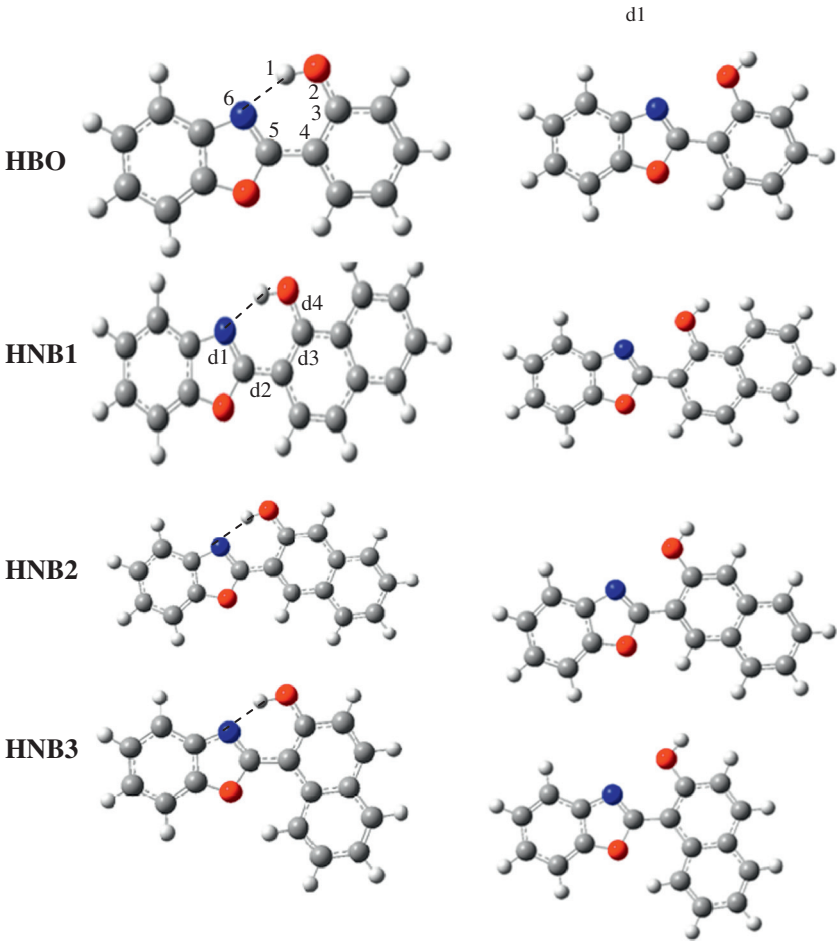

Fig. 1. The closed H-bonded and open non-H-bonded structures of **HBO** and **HNB1–3**.

ger resonance with the H-bonded ring leads to more localized π-electron structure.

Table 1 presents the estimated H-bonding energies, ΔE_{HB}, of the **HBO** and **HNB1–3** computed by comparing the energies of the closed (H-bonded) and the open E forms, the later is obtained by 180° rotation of the OH around the C–O bond. The H-bonding energies of HBO and **HNB1–3** at the S_0–E state are 11.9, 14.0, 11.2 and 15.5 kcal/mol, in good agreement with the calculated H-bonding distances. At the S_1–E state, these energies are 12.4, 15.0, 8.6 and 16.4 kcal/mol, respectively. By comparing the H-bonding energies, it can be predicted that upon photoexcitation to the FC region, the strength of H-bonding in **HNB2** reduces, indicating a competition between amount of delocalization of π-electron and the strength of H-bonding.

Ground and excited states potential energy curves

Fig. 3 illustrates the potential energy curves along the proton transfer (PT) pathway in the ground and excited states as a function of the reaction coordinate for **HBO** and **HNB1–3.** Apart from constraining the O–H distance, we relaxed all other degrees of freedom without imposing any symmetry constraints during the geometry optimization. To investigate the proton transfer through the IMHB process, we have defined a reaction coordinate (RC) as the difference between breaking OH and forming NH bonds (RC = d(OH) − d(NH). As can be seen, the potential energy surface (PES) at the S_0 state is strongly asymmetric in favor of the O–H···N H-bond. Inspection of the Fig. 3 reveals that at the S_0 state of **HBO** and **HNB1–3**, enol (S_0–E) forms with OH···N H-bonding are the most stable tautomeric forms. As can be seen, there is no a deep minimum on the potential energy surface of the K forms at the S_0 state. The repulsive nature of the ground state PE curve outright discards any chance of the ground state intramolecular proton transfer at the S_0 state. Thus K forms in the related S_0 states are not stable. They are converted to the E form during the optimization. However, as can be seen in Fig. 3, measure of the stability of the K forms for **HNB1–3** isomers is not equal. In the case of **HNB1–3** molecules, tautomers are associated with a reorganization of π-electron structure. As a result of possibility of cooperative interaction between H-bonding formation and an increase of π-electron delocalization, it is estimated that the K form of **HNB1** to be most stable isomer with respect to the other K forms.

Very interesting is the simple enaminone and ketohydrazone systems including N–H···O H-bonding are more stable than their iminoenol and azoenol ones having O–H···N, owing to the greater proton affinity of nitrogen with respect to oxygen [56]. Our results show that the stability order is reversed if a naphthalene moiety is fused with the H-bonded ring because the formation of the N–H···O tautomer in ground state leads to the loss of large resonance energy in benzene and naphthalene rings. Thus, O–H···N tautomer of **HBO** and **HNB1–3** becomes the more stable one after fusion of the H-bonded ring with a benzene and naphthalene moieties.

The instability of the K forms with respect to the E forms as well as high energy barrier for E to K transformation (approximately, between 8.0 and 15.0 kcal/mol) on the ground state potential energy surface discards any opportunity of the ground state intramo-

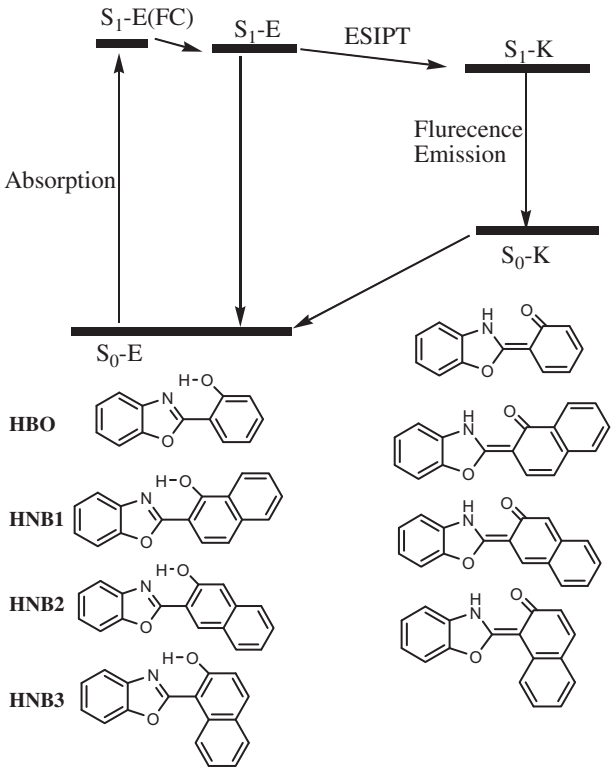

Fig. 2. Energy diagram of phototautomerization for **HBO** and **HNB1–3**.

Table 1
Relative energy (kJ/mol) of **HNB1–3** molecules and at H-bonding energies (kcal/mol), ΔE_{HB}, at PBE1PBE/6-311++G(2d,2p) level of theory.

	HNB1	HNB2	HNB3
ΔE_{ele}	0.00	9.50	17.16
ΔE_0[a]	0.00	8.91	16.76
ΔE[b]	0.00	8.52	16.36
ΔH	0.00	8.52	16.36
ΔG	0.00	7.79	15.29
$\Delta E_{HB}(S_0)$	14.0(11.9)[c]	11.2	15.5
$\Delta E_{HB}(S_1)$	15.0(12.4)[c]	8.6	16.4

[a] $\Delta E_0 = \Delta E_{ele} + \Delta ZPE$.
[b] $\Delta E = \Delta E_0 + \Delta E_{thermal}$.
[c] For **HBO**.

lecular proton transfer (GSIPT) process thermodynamically and kinetically.

Proton transfer in the process of conversion E to K causes the structural changes in the **HBO** and **HNB1–3**. We have examined how the structural parameters are affected by the proton transfer by performing optimization of structures on the potential energy surfaces. Variations of d(N–H), d(O–H), d(O···N) and O–H···N angle versus RC along the PT pathway in **HNB1** is illustrated in Fig. 4 and those of **HBO** and **HNB2–3** are shown in Figs. S1–2 (as Supplementary data). The PT from O–H···N to O···H–N is associated with the increase of the O–H and decrease of N···H distances. These figures show that the O···N distance first decreases, then passes through a minimum, and finally increases before relaxing to the K form. In addition, variation of O–H···N angle with RC reveals that in contrast to the O···N distance it first increases, then passes through a maximum, and finally decreases before relaxing to the K form. Thus, O···N distance contracts to a minimum and O–H···N angle increases to a maximum before the PT process is completed. From Figs. 4a and S1, it is obvious that the H···N and O···N distances decrease as the E form approaches transition state (TS). This distortion in the molecules on going from GS to TS takes

Table 2
Selected structural parameters (Å and °) calculated at PBE1PBE/6-311++G(2d,2p) level of theory.

	HNB1			HNB2		
	S_0–E	S_1–E	S_1–K	S_0–E	S_1–E	S_1–K
O–H	0.989	1.014	1.798	0.982	1.051	1.831
d_1	1.304	1.330	1.341	1.300	1.335	1.346
d_2	1.436	1.412	1.418	1.442	1.409	1.418
d_3	1.395	1.448	1.456	1.432	1.449	1.469
d_4	1.329	1.316	1.259	1.340	1.302	1.263
N–O	2.610	2.563	2.591	2.642	2.490	2.604
N–H	1.719	1.627	1.030	1.759	1.510	1.026
N–H–O	147.8	151.3	151.3	147.6	152.5	129.3
	HNB3			**HBO**		
O–H	0.997	1.008	1.582	0.985	1.034	1.835
d_1	1.309	1.339	1.346	1.302	1.340	1.340
d_2	1.444	1.408	1.414	1.440	1.410	1.433
d_3	1.406	1.469	1.488	1.411	1.456	1.453
d_4	1.326	1.318	1.264	1.334	1.309	1.269
N–O	2.526	2.518	2.474	2.632	2.529	2.609
N–H	1.626	1.592	1.057	1.749	1.569	1.027
N–H–O	147.9	150.3	138.4	147.3	152.2	129.2

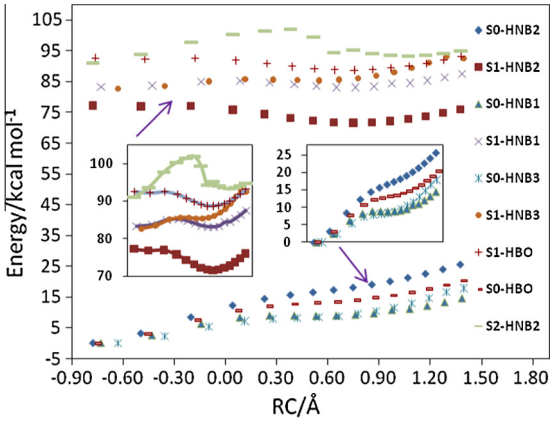

Fig. 3. Potential energy curves along the proton transfer (PT) pathway at the ground and excited states as a function of the reaction coordinate (RC) for **HBO** and **HNB1–3**.

place in order to approach the H-donor and H-acceptor atoms for the occurrence of the PT reaction.

The potential energy curve along the ESIPT pathway at the excited (S_1) states of **HBO** and **HNB1–3** as a function of the reaction coordinate RC = [d(OH) − d(NH)] are depicted in Fig. 3. Information on the ESIPT mechanism was obtained by calculating the Franck–Condon (FC) transition energies at the TD-DFT (PBE1PBE)/6-311++G(2d,2p) using the PBE1PBE/6-311++G(2d,2p) ground state structures. The Franck–Condon (FC) curves for the proton transfer processes were calculated by adding the TD-DFT excitation energies to the corresponding GSIPT curves. These figures show the change in the stability pattern of tautomers upon electronic excitation. As can be seen, ESIPT curves at the excited (S_1) state shows two minima corresponding to the S_1–E and S_1–K forms at the R(O–H) = 1.034 and 1.835 Å for **HBO**, 1.014 and 1.798 Å for the **HNB1**, 1.051 and 1.831 Å for the **HNB2** and 1.008 and 1.582 Å for the **HNB3**. The R(O–H) of second minimum found in the **HNB3** is smaller than others. The energy difference between the two minima obtained on the PES of **HBO** and **HNB1–3** is estimated to be −3.9 kcal/mol and −0.1, −5.1 and 2.7 kcal/mol, respectively. On the other hand, the energy difference between two optimized S_1–E and S_1–K forms is 15.2 kcal/mol for **HBO** and 9.3, 16.9 and

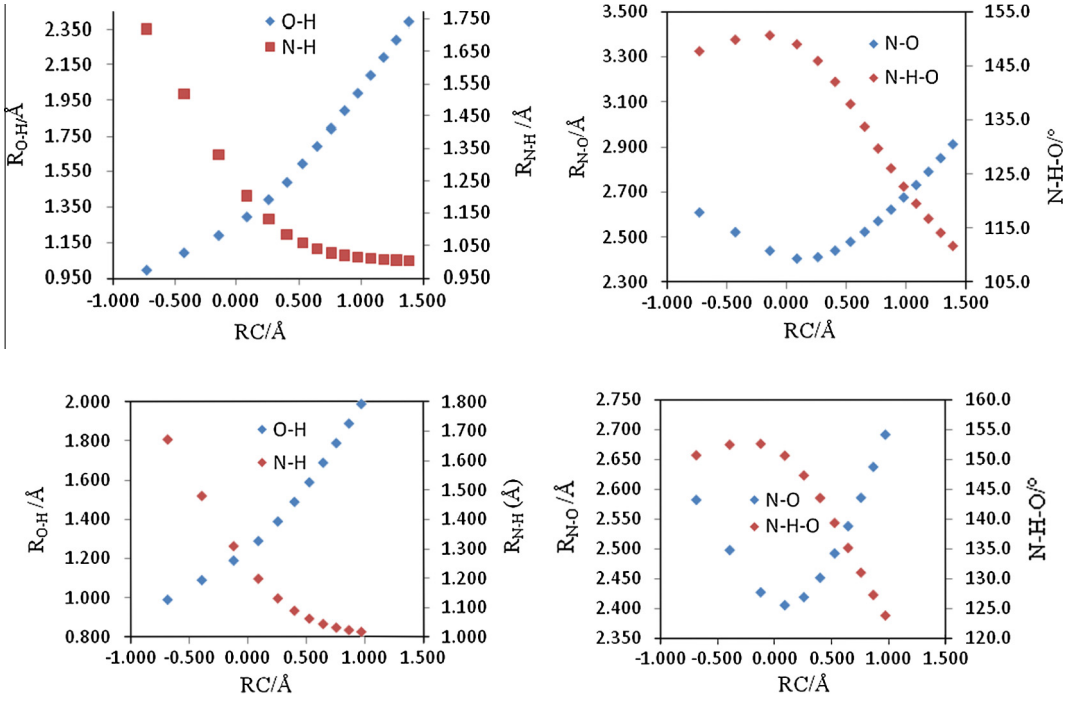

Fig. 4. Variation of O–H, N–H and N–O distances and N–H–O angle against PT reaction coordinate (RC) for **HBO** at the S_0 (a) and S_1 (b) states.

6.7 kcal/mol for **HNB1–3**, respectively. Comparing **HNB1** and **HNB3** with **HBO**, it seems the proton transfer of **HBO** is more endergonic than **HNB1** and **HNB3**, due to more energy is estimated to require for destroying the aromaticity of benzene ring than naphthalene ring in **HNB1** and **HNB3**. The trend is opposite for **HNB2** with respect to the **HBO.**

In the S_1 state, there is a barrier separating the S_1–E and S_1–K tautomers. The energy barrier for the conversion S_1–E to S_1–K at the excited state is predicted to be minor (≈0.3 kcal/mol for **HBO** and 0.4, 1.9 and 3.1 kcal/mol for **HNB1–3**, respectively). The S_1–E for **HBO** and **HNB1–3** lies 83.0, 75.1, 63.9 and 73.8 kcal/mol above the S_0–E and 9.5, 6.1, 13.3 and 8.8 kcal/mol below the Franck–Condon point that is reached initially upon vertical photoexcitation to the S_1 state. Hence, access to S_1–K should be facilitated, because the small energy barrier should easily be overcome by the energy gained during the relaxation process from the Franck–Condon point to S_1–E.

For our studied molecules, although barrier heights are small but the existence of these barriers will retard the formation of the S_1–K states and reduce the yields of the S_1–K states. Interestingly, although the calculated energy difference between the S_1–E form and S_1–K form obtained during vertical excitation of **HNB3** is positive and energy barrier for ESIPT reaction is greatest, experimental work of Iijima et al. [41] showed dual fluorescence for **HNB3** in benzene with peak maxima at 400 and 460 nm. Thus, according to the nature of the S_1 PE curves and difference in peak wavelength between absorption and emission (will be dealt with in Excitation and emission energies) as well as low energy barrier for the PT reaction at the S_1 state, conversion S_1–E to S_1–K is estimated to be possible in good agreement with the experimental results. The similar situations have been observed for 7-hydroxy-1-indanone fused by benzene and naphthalene rings [57] that S_1–K forms have greater energy than S_1–E ones. Therefore, in contrast to the S_0 ground state, K form of **HBO** and **HNB1–3** can be formed at the S_1 state.

Our findings brought up a question: Why do the energy barriers follow the order **HBO** ≈ **HNB1** < **HNB2** < **HNB3**. To answer this question we consider change in the interannular bond length ($\Delta d2 = d2(S_1\text{–E}) - d2(S_0\text{–E})$) upon S_0–E to S_1–E conversion. The d2 bond was defined in Fig. 1. The ($\Delta d2$) value is −0.03 Å for **HBO** and −0.024, −0.033 and −0.035 Å for **HNB1–3**, respectively, in agreement with the order of the calculated energy barrier for **HNB1–3**. Decrease in d2 of the S_1–E also decreases O···N distance between donor and acceptor proton units.

As mentioned above, we found two stationary points of the S_1–E and S_1–K forms at the S_1 state so that the first minimum on the PES is correlated to the S_1–E form. The structural changes upon S_0–E → S_1–E conversion can be judged from Table 2. Upon photoexcitation to the first singlet excited state (S_1), the OH group of **HBO** and **HNB1–3** becomes more acidic and the nitrogen atom becomes more basic, relative to those in its ground state, thereby inducing ESIPT. As seen in Table 2, decrease in O···N and H···N distances, increase in O–H bond length and O–H···N bond angle upon photoexcitation are some structural changes in accord with transfer of proton from OH moiety to the N atom of proton transfer ring at the S_1 state. The other important bond lengths that change upon photoexcitation are d1, d2, d3 and d4. During the S_0–E → S_1–E process, the O–H bond weaken and the H···N H-bond strengthened, causing the d1 and d3 bonds elongated, thereby decreasing their double bond character and d2 and d4 ones shortened significantly, giving them more double bond character. The shortening of the central d2 bond during the photoexcitation decreases H···N H-bond, thereby promote the occurrence of the ESIPT process and inhibit the internal rotation of the benzoxazole ring at the S_1 state.

During the ESIPT (S_1–E → S_1–K) process, comparing the structural parameters of the E with K reveals that how the molecular structures are transformed. Although, structure of the K form of **HBO** and **HNB1–3** at the S_1 state also has a C_s symmetry, structures of S_1 state (E and K forms) and minimum structure of S_0 are qualitatively different because H1 atom that is bonded to the O atom in the S_0 state is attached to the N atom in the S_1 state. As illustrated in Fig. 3, E forms of molecules are global minimum at the S_0 state, while they are less stable in the S_1 state and are converted to K form during excitation due to their low barrier PES for ESIPT. Thus,

E to K tautomerization at the S_1 state can be the main decay channel for **HBO** and **HNB1–3** in the gas phase after the singlet state S_1 is populated. Figs. 4b and S2 illustrate the variations of d(N–H), d(O–H), d(O···N) and O···H···N angle versus RC along the PT pathway of the **HBO** and **HNB1–3** compounds in the S_1 state. Similar to the S_0 state, the PT from OH to N atom of ring is associated with the decrease of the H···N distance and increase of O–H bond. As can be seen, O···N distance decreases to a minimum and O···H···N angle increases to a maximum before the transfer of proton occurs from OH to N atom of benzoxazole ring completely. The crossover point (COP) between E– and K forms of **HNB1–3** lies at RC ≈ 0.091, 0.095 and 0.113 Å, respectively. At the COP, the O···N distance has lowest amount and the O–H bond character is exchanged by N–H bond character. The ESIPT mechanism can be illustrated in three consecutive steps associated with the three regions, viz., before the COP, in COP and after COP. In the first step, O···N and H···N distances decrease while O–H bond length increases. The O···N distance at the COP of **HNB1–3** is 2.407, 2.391 and 2.395 Å, respectively. This distortion in the structure of **HNB1–3** takes place in order to facilitate the occurrence of the PT reaction in the S_1 state. Finally, O···N distance increases and H atom remains with the N atom.

Although plots in Figs. S1 and S2 show similar trends in the variations of d(O···N) distance and O···H···N angle versus RC in the S_0 and S_1 states, but value of O···N distance is different in COP of two states. In contrast to the **HNB2**, the O···N distance in COP of S_1 state for **HNB1** and **HNB3** is greater than that of S_0 one. Thus COP in the S_1 state of **HNB1** and **HNB3** takes place at longer O···N distance.

Excitation and emission energies

Since main focus in the present work is on ESIPT reaction of **HBO** and **HNB1–3** in the S_1 state, we only discuss the vertical excitation and emission energies to the lowest excited singlet state (S_1). We have employed time-dependent density functional theory (TD-DFT) to investigate the first singlet excited state behavior of **HNB1–3** and parent compound of our study, 2-(2′-hydroxyaryl)benzoxazole (**HBO**). The calculated spectroscopic data are given in Tables 3 and S1 (as Supplementary data).

Upon photoexcitation to the S_1 state, the Franck–Condon excited state is relaxed to the minimum of the first excited state S_1–E. Two decay mechanisms can be proposed for S_1–E molecules. These molecules may emit photon and fall to the ground state S_0–E or undergo tautomerization via ESIPT and be converted to the S_1–K one. As can be seen in Table 3, S_1–E to S_0–E transition peaks are appeared at the greater wavelengths with respect to the excitation wavelengths. In the second decay mechanism, K form produced upon ESIPT process is returned to its ground state (S_0-K) accompanied by fluorescence emission and then by a reverse hydrogen transfer in the ground state is converted to S_0–E.

The calculated excitation and emission energies of transitions at PBE1PBE/6-311++G(2d,2p) level in the gas and aqueous phases are given in Table 3. As can be seen, first vertical excitation energies (VEE) calculated for **HBO** and **HNB1–3** in the gas phase at PBE1PBE/6-311++G(2d,2p) level of theory are 32493.3, 29201.7, 27,096 and 28999.3 cm^{-1}.

The calculated absorption wavelength of **HNB3** (346.2 nm) is in good agreement with that of experimental value (361.0 nm) [41]. This agreement confirms the validity of PBE1PBE/6-311++G(2d,2p) level of theory in the prediction of the photophysical parameters of **HBO** and **HNB1–3**. The VEE calculated for **HNB2** in the gas phase is smaller than those of **HNB1** and **HNB3**. Consequently, the energy difference between two electronic levels involved in transition is lower in **HNB2** than others.

In general, extension of the aromatic ring structure leads to the decrease in the energy gap between the ground and excited states and in turn red shift in both absorption and fluorescence bands. As can be seen, absorption bands of **HNB1–3** are appeared at longer wavelengths than that of 2-(2′-hydroxyaryl)benzoxazole (**HBO**) (308.96 nm and exp. value of 335 nm [41]). Thus, absorption bands of **HNB1–3** in gas phase are red shifted with respect to those of **HBO**, indicating that the insertion of aromatic ring to the **HBO** produces a batochromic effect on the absorption spectrum of **HBO**. The red shift in the absorption bands of **HNB1–3** with respect to the **HBO** is 34.9, 61.6 and 37.3 nm, respectively. A comparison between red shift values of **HNB1–3** shows that their values depend on the position of inserted aromatic ring and the degree of the delocalization of π electrons. In other words, there is a correlation between the degree of delocalization of π electrons in the conjugated system and the value of red shift in absorption wavelength. Accordingly, influence of the extension of π conjugation on the wavelength of absorption band and in turn decrease in the energy gap between the ground and excited states of the **HNB2** is major.

The oscillator strengths, *f*, for $S_0 \rightarrow S_1$ absorption bands of **HBO** and **HNB1–3** appeared at 308.9, 343.8, 370.5 and 346.2 nm are 0.4210, 0.043, 0.3745 and 0.4356, respectively. If we compare the position and oscillator strength of the $S_0 \rightarrow S_1$ band of **HBO** with those of **HNB1–3**, we can observe that the intensity of the $S_0 \rightarrow S_1$ absorption band decreases and increases on going from **HBO** to **HNB1–2** and **HNB3**, respectively.

The calculated S_1–K → S_0–K fluorescence emission energy of **HNB1–3** in the gas phase is 23273.8, 14783.9 and 25024.4 cm^{-1} at the PBE1PBE/6-311++G(2d,2p) level of theory. As mentioned above, photophysical properties of molecules depend not only on the size of the π-conjugated system, but also on the relative position of the annulated ring extension. Thus, interplay between aromaticity and effective π-conjugation length on the photophysical

Table 3
Vertical excitation energies (VEE), dipole moments, absorption and emission wavelengths, oscillator strengths (*f*) and fluorescence rate constants (k_f) in the two phases at PBE1PBE/6-311++G(2d,2p) level of theory.

	HNB1(gas)			HNB1(water)			HNB2(gas)			HNB2(water)		
	S_0–E	S_1–E	S_1–K	S_0–E	S_1–E	S_1–K	S_0–E	S_1–E	S_1–K	S_0–E	S_1–E	S_1–K
VEE1/kcal/mol	83.2	75.1	66.3	82.6	69.8	63.6	77.2	63.9	42.1	78.9	65.7	45.5
μ/D	1.5	1.3	4.7	2.3	1.8	6.3	2.6	3.0	7.0	3.7	3.9	10.0
λ1/nm	343.8	380.9	431.4	346.1	409.7	449.4	370.5	447.6	679.1	362.3	434.9	627.7
*f*1	0.375	0.361	0.373	0.503	0.925	0.750	0.043	0.045	0.065	0.050	0.102	0.151
k_f (s^{-1})/10^8			1.300			2.500			0.093			0.260
	HNB3(gas)			**HNB3**(water)			**HBO**(gas)			**HBO**(water)		
VEE1/kcal/mol	82.6	73.8	71.3	81.7	67.3	66.6	92.5	83.0	63.5	92.4	76.3	64.0
μ/D	1.8	1.7	3.5	2.7	2.5	5.1	2.2	2.2	5.8	3.1	2.6	7.9
λ1/nm	346.2	387.6	401.2	349.9	424.6	429.4	309.0	344.4	450.0	309.4	374.9	446.5
*f*1	0.436	0.472	0.354	0.551	0.888	0.666	0.421	0.381	0.207	0.600	1.090	0.497
k_f/10^8			1.500			2.400			0.683			1.680

properties of studied molecules can be observed. The emission energy for **HNB3** is in reasonable agreement with the experimentally measured value of 460 nm [41]. The $S_1 \rightarrow S_0$ emission wavelength of **HBO** in the gas phase (450 nm and exp. value of 508 nm) is smaller than related values in **HNB1** (431.4 nm) and **HNB3** (401.2 nm). Therefore, as reported by Iijima et al. [41], in these cases, extension of the aromatic ring structure increases the energy gap between K forms of ground and excited states. As reported by Iijima et al. [41], mechanism of this effect still remains unknown. For **HNB2**, situation is opposite, meaning that the extension of the aromatic ring structure decreases the energy gap between ground and excited states of K form and consequently increases emission wavelength of radiation by 229.1 nm on going from **HBO** to **HNB2**. It should be noted that the red shift observed in both absorption (61.6 nm) and emission bands of **HNB2** upon extension of π conjugation with respect to the **HBO** is remarkable. Although transition probability for $S_0 \rightarrow S_1$ transition is small ($f = 0.043$), but the extension of π conjugation in **HNB2** leads to the better delocalization of the π electrons at the excited state S_1 and in turn decrease in energy of S_1–K. The greater decrease in energy of the S_1–K of **HNB2** with respect to the others can be considered as a driving force for the ESIPT process. The calculated $S_0 \rightarrow S_2$ absorption energy of **HNB2** in the gas phase is 31826.9 cm^{-1}. The $S_0 \rightarrow S_2$ absorption band is of comparatively higher intensity and involves an excitation from the HOMO-1 to the LUMO. The results of calculations showed that the transition probability for $S_0 \rightarrow S_2$ absorption transition ($f = 0.7102$) in **HNB2** is greater than $S_0 \rightarrow S_1$ ($f = 0.0430$). Nevertheless, $S_1 \rightarrow S_0$ ($f = 0.0646$) is the most probable emission in the fluorescence spectrum of the K form of **HNB2**.

Fig. S3 in Supplementary data shows the variation of the oscillator strength, *f*, of FC transitions versus RC on going from E form to the K one at the ground state S_0. For **HBO**, **HNB1** and **HNB3**, it is observed that the *f* value first decreases and then increases on going from S_1–E form to the S_1–K one, while for **HNB2**, *f* value increases continually. Comparison of the *f* values shows that the intensity of fluorescence emission for **HNB2** is smaller than others.

All three isomers and parent compound **HBO** exhibit Stokes-shifted fluorescence. The calculated Stokes shift for **HBO** is from 308.9 to 450.0 nm and those of **HNB1–3** are from 343.8 to 431.4 nm, 370.50 to 679.1 nm and 346.2 to 401.2 nm at PBE1PBE/6-311++G(d,p) level of theory. Therefore, Stokes shift values are 141.1 nm for **HBO** and 87.6 nm, 308.6 nm and 55.0 nm for **HNB1–3**, respectively. These Stokes shifts make E to K photoswitching possible. As expected from these values and PE curves given in Fig. 3, Stokes shift for **HNB2** is greater than others. As a result, potential of **HNB2** molecule as an emissive and electron transport material in designing improved organic white light emitting diodes is predicted.

Effect of solvent

Solvent molecules can affect not only the structural equilibrium of species but also their absorption and fluorescence spectra. As can be seen in Table 3, the vertical S_0–E → S_1–E transition leads to minor decrease of the dipole moment of all molecules with the exception of **HNB2** that increases from 2.590 to 3.026 D. As can be seen, dipole moment only increases on going from **HBO** to **HNB2** at the both states, indicating a considerable charge redistribution induced by extension of aromatic ring in this molecule. Besides, S_1–E → S_1–K phototautomerization process leads to a considerable increase of the dipole moment.

As the results listed in Table 3 show, increase in polarity of the solvent is accompanied by a progressive red shift of the absorption and fluorescence spectra in the **HBO**, **HNB1** and **HNB3** with the exception of **HNB2** that exhibited a blue shift. These changes are more manifested in the emission than in the absorption spectra. The results obtained in both gas and solution phases show a correlation between change in the dipole moment on going from ground state to excited state and amount of Stokes shift. The more dipole moment change is observed, the more Stokes shift is resulted. An increase in the Stokes shift is observed by increase in polarity of solvent in the **HBO**, **HNB1** and **HNB3**, but there is an exception for **HNB2**. Nevertheless, Stokes shift in both gas and liquid phases is greater for **HNB2** (308.6 nm and 265.4 nm) than others. It is also resulted that the emission spectrum of **HNB2** is more sensitive to solvent properties so that achieving a white light is much facilitated in solvents with less polarity.

We have also calculated the fluorescence rate constant, k_f(in s^{-1}), for phototautomeric (S_1–K) forms by using Einstein's emission transition probability equation [58,59]:

$$k_f = f \times \nu(\mathrm{cm}^{-1})/1.5$$

where ν is fluorescence wavenumber and *f* is the oscillator strength. The calculated fluorescence rate constants are given in Table 3. The calculated k_f values are arranged as **HNB3** > **HNB1** > **HBO** > **HNB2**. As can be seen, k_f increases by raise in polarity of solvent and for **HNB2** in both phases is smaller than other molecules.

The radiative lifetime ($\tau = 1/k_f$) of phototautomeric form, S_1–K, of **HBO** and **HNB1–3** molecules were calculated to be 14.7, 7.5, 107.0 and 6.8 ns in the gas phase and 6.0, 4.0, 39.2 and 4.15 ns in the water, respectively. It can be predicted that the radiative lifetime decreases as the phase change from gas to water. The results also show that the τ(**HNB2**)/τ(**HNB1**) = 14.3 and τ(**HNB2**)/τ(**HNB3**) = 15.7 in gas phase. Therefore, fluorescence quantum yield is estimated to be greater for **HNB2** than other two isomers.

The Frontier molecular orbital analysis

As expected, upon excitation of S_0–E to the first singlet excited state (S_1) and in turn redistribution of charge density, the proton donor OH group of **HNB1–3** molecules become more acidic and the proton acceptor nitrogen atom becomes more basic, relative to those in its ground state. The results show that the vertical $S_0 \rightarrow S_1$ transition in the Frank–Condon region of **HNB1–3** molecules corresponds essentially to the excitation from HOMO (π) to LUMO (π*), which are mostly located in different parts of the molecule. In the following, we preferentially focus on the electron density projection over the PT (IMHB) ring. Analysis of the HOMO (Fig. S5 in Supplementary data) within IMHB ring reveals that the HOMO in the S_0–E and S_1–E forms of all molecules (**HBO** and **HNB1–3**) is a π orbital with bonding character across OH, d3(C3–C4) and d1(C5–N6) bonds and antibonding character across d2(C4–C5) and d4(C3–O) bonds with the exception of **HNB2.** The HOMO at the S_1–E and S_2–K states of **HNB2** has different characteristic. As can be seen, S_0 to S_1 transition is accompanied by a transfer of negative charge from the phenol ring to the benzoxazole ring that affect on the transfer of proton in the same direction.

As can be seen in Fig. S5, the LUMO is a π* orbital with bonding character centered along the d2 bond axis and antibonding character located along the O–H, d1, d3 and d4 bond axes. As can be seen, upon electronic excitation from HOMO to LUMO at the S_0–E state, electron density on the O atom decreases and that of the N atom increases. In addition, excitation of electron leads to depletion of electron density at the O–H bond and in turn weakness of it. Thus, upon excitation of electron from HOMO to LUMO in the Franck–Condon region, the hydroxyl proton is expected to be more acidic, whereas the N atom is estimated to be more basic with respect to the ground state, which will facilitate or even trigger the subsequent transfer of proton.

During the S_1–E → S_1–K process, the O–H bond of molecules weaken and the H···N H-bond strengthened, causing the d1 and

d3 bonds to be elongated and d2 as well as d4 bonds to be shortened. The changes in bond lengths upon photoexcitation are resulted from the π-electron density transition from the highest occupied molecular orbital (HOMO) to the lowest unoccupied molecular orbital (LUMO). After the HOMO to LUMO transition, the π-bonding character of the d1 and d3 bonds decreased; therefore, these bonds were elongated. In contrast, the π-bonding character of the d2 and d4 bonds increased, thereby shortening the C1–C2 bond and consequently decreasing the H···N distance were resulted. In contrast to projection of electron density in LUMO of **HBO**, **HNB1** and **HNB3**, O atom has no electron density population in LUMO of all forms of **HNB2**.

As can be seen in Fig. S5, HOMO of the K form within IMHB ring of all studied molecules is a π orbital composed of bonding contributions mainly along the d1 and d3 bonds axes along with large electron density on the carbonyl oxygen. The antibonding contributions of HOMO are located across d2 and d4 bonds. The LUMO is also a π* orbital with bonding character centered along the d2 bond axis and antibonding characters located along the d1, d3 and d4 bond axes. Upon electronic excitation from HOMO to LUMO, electron density on the O atom decreases and that of the N atom increases. In addition, HOMO frontier orbital analysis reveals that the location of electron density population at the S_1–K form of **HNB2** is the same of S_1–E one. The presence of antibonding contributions along the d1, d3 and d4 prevents the electron delocalization in the aromatic nucleus and thereby forbids the reverse PT from K form to E one at the S_1 state.

Population analysis

The occurrence of ESIPT implies that a certain amount of electronic charge is transferred between proton acceptor moiety and proton donor one by photoexcitation. The CHelpG population analysis data calculated at MP2/6-311++G(d,p)//PBE1PBE/6-311++G(d,p) level of theory are given in Table 4. For several typical H-bonded systems, it has been demonstrated that the charge is transferred from the proton acceptor to the proton donor [60]. As can be seen in Table 4, the charge on the O atom involved in IMHB of **HBO** and **HNB1–3** in the $S_0(S_1)$–E states are −0.5531 (−0.5589) au and −0.4940 (−0.5038) au, −0.5529 (−0.5662) au and −0.5693 (−0.5680) au, respectively. By comparing the charges of the O atom for **HNB1–3** molecules at both S_0–E and S_1–E states, it can be seen that the negative charge of the O atom increases on going from **HNB1** to **HNB3**. Besides, extension of the aromatic ring changes the negative charge of the O atom so that their effects are different. The negative charge of O atom at the both states is greater for **HNB3** than others. The greater negative charge of O atom in **HNB3** facilitates the proton transfer from O to N atom. Upon photoexcitation from S_0–E to S_1–E, the negative charge of N atom in all molecules decreases and the negative charge of O atom in all molecules increases with the exception of **HNB3**. These changes in negative charge of N and O atoms is greater for **HNB2** (0.0627 au for N and 0.0134 au for O) than others. The positive charge of H atom at the both S_0–E and S_1–E states increases on going from **HNB1** to **HNB3**.

Table 4
CHelpG population analysis data (in au) calculated at MP2/6-311++G(2d,2p)//PBE1PBE/6-311++G(2d,2p) level of theory.

	HNB1			**HNB2**		
	S_0–E	S_1–E	S_1–K	S_0–E	S_1–E	S_1–K
q_N	−0.4774	−0.4652	−0.4762	−0.4799	−0.4172	−0.4880
q_H	0.3387	0.3410	0.4301	0.3449	0.3442	0.4443
q_O	−0.4940	−0.5038	−0.6324	−0.5529	−0.5662	−0.7387
CT	0.0291	0.0486	0.5081	0.0523	0.0736	0.6242
	HNB3			**HBO**		
q_N	−0.4975	−0.4907	−0.5925	−0.4808	−0.4404	−0.4889
q_H	0.3788	0.3816	0.4962	0.3494	0.3434	0.4457
q_O	−0.5693	−0.5680	−0.6967	−0.5531	−0.5589	−0.7235
CT	0.0736	0.0566	0.5655	0.0355	0.0424	0.5678

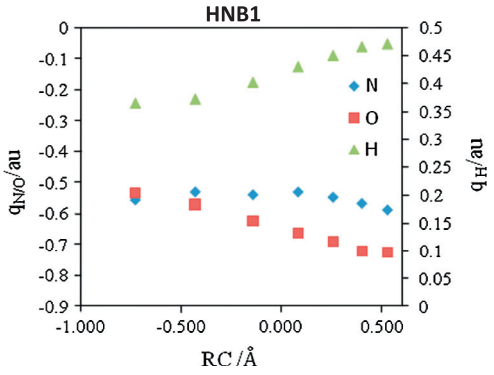

Fig. 5. The variation of the charge on the atoms involved in PT reaction (N, O and H) in **HNB1** with RC.

The charge of the benzoxazole moiety of **HBO** and **HNB1–3** can be considered as a measure of charge exchanged between two parts of molecules. The charge transfer values (CT) are given in Table 4. The positive charge of benzoxazole ring (CT values) confirms that the charge in the both S_0–E and S_1–E states is transferred from benzoxazole ring to proton donor one. The CT values at the S_0–E state increases on going from **HNB1** to the **HNB3**. Upon photoexcitaion from S_0–E to S_1–E, CT value for all molecules increases with the exception of **HNB3**. From these data, it can be estimated that the $S_0E \rightarrow S_1$–E transition is accompanied by a partial charge transfer from the benzoxazole ring to proton donor ring in **HBO** and **HNB1–2**. An opposite trend is predicted for **HNB3**. Besides, exten-

Table 5
Topological properties of the electron density (au) at PBE1PBE/6-311++G(2d,2p) level of theory in the ground state.

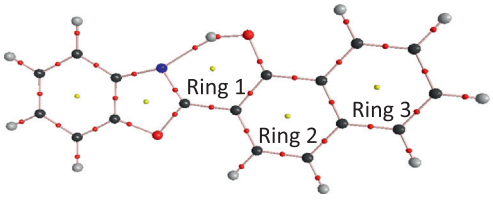

	HNB1			**HNB2**		
	$\rho(r)$	$\nabla^2\rho(r)$	H(r)	$\rho(r)$	$\nabla^2\rho(r)$	H(r)
O–H	0.3379	−2.5473	−0.7079	0.3462	−2.6233	−0.7273
N···H	0.0496	0.1099	−0.0082	0.0449	0.1094	−0.0056
d_1	0.3768	−1.2640	−0.5522	0.3796	−1.2736	−0.5636
d_2	0.2884	−0.7850	−0.2769	0.2855	−0.7719	−0.2699
d_3	0.3122	−0.8851	−0.3220	0.2913	−0.7751	−0.2761
d_4	0.3167	−0.6035	−0.5023	0.3114	−0.6325	−0.4886
Ring1	0.0197	0.1183	0.0043	0.0186	0.1101	0.0041
Ring2	0.0226	0.1522	0.0058	0.0230	0.1539	0.0058
Ring3	0.0237	0.1590	0.0058	0.0235	0.1573	0.0058
	HNB3			**HBO**		
O–H	0.3298	−2.4444	−0.6863	0.3435	−2.5985	−0.7208
N···H	0.0624	0.1149	−0.0155	0.0461	0.1097	−0.0062
d_1	0.3730	−1.2472	−0.5394	0.3786	−1.2705	−0.5592
d_2	0.2824	−0.7438	−0.2657	0.2866	−0.7775	−0.2728
d_3	0.3050	−0.8381	−0.3066	0.3027	−0.8342	0.3005
d_4	0.3200	−0.6252	−0.5098	0.3140	−0.6250	-0.4951
Ring1	0.0210	0.1286	0.0045	0.0190	0.1127	0.0042
Ring2	0.0223	0.1501	0.0058	0.0237	0.1597	0.0058
Ring3	0.0237	0.1587	0.0058			

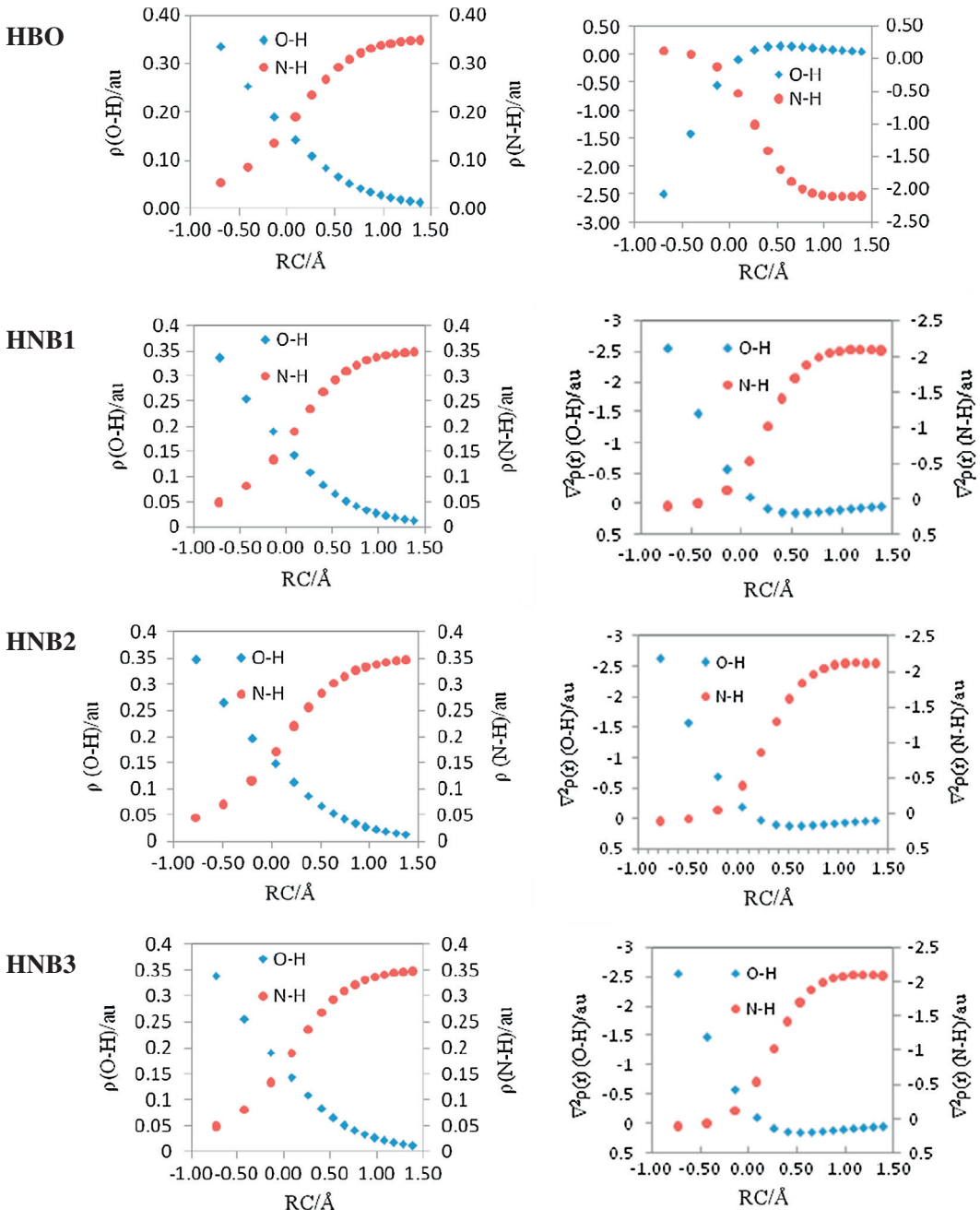

Fig. 6. Variation of electron density and Laplacian of electron density $\nabla^2\rho(r)$ at the N(O)–H BCP versus RC along the PT pathway of the **HBO** and **HNB1–3** at the S_0 state.

sion of the aromatic ring results in increase of CT value at the S_1–E state.

In the PT process, the positively charged proton is transferred from the proton donor ring to the benzoxazole ring. After PT, the benzoxazole ring of the S_1–K form obviously becomes more positive and O atom becomes more negative with respect to the corresponding S_0–E and S_1–E forms. As can be seen, negative charge of O atom in the S_1–K form and positive charge of the benzoxazole ring in both S_1–E (0.0736 au) and S_1–K (0.6242 au) forms of **HNB2** is greatest. Thus, redistribution of electron density in the **HNB2** upon phototatomerization is more significant than other molecules. This can be a possible explanation of the greater Stokes shift observed for **HNB2**.

The variations of the charge of atoms involved in PT reaction (N, O and H) with RC for **HNB1** (Fig. 5) and those of **HBO** and **HNB2–3** in ground state are illustrated in Fig. S4 (as Supplementary data). In all molecules, negative charge of oxygen atom and positive charge of H atom during OH···N to O···HN PT reaction increases. The change in negative charge of the N atom is lower than O atom for all studied species during E to K conversion.

AIM analysis

The quantum theory of atoms in molecules (QTAIM) is a useful tool to characterize hydrogen bonding. One of the advantages of the AIM theory is that one can obtain information on changes in the electron distribution as a result of either bond formation or complex formation [41–43,61,62]. Recently AIM analysis has been used to characterize the H-bonds involved in PT process [33,63,64]. The molecular graphs (including the critical points and bond paths)

of the E and K forms of molecules are shown as Supplementary data in Fig. S6. In addition to all of the expected BCPs, the electron density analysis reveals an additional BCP in OH···N (E form) and NH···O (K form) distances and a ring critical point in IMHB region.

AIM method can be a great help for assessing the variations in chemical bond nature occurring along the PT pathway. In proper HBs, formation of the Y···H–X H-bond is accompanied by a weakening of the covalent H–X bond with concomitant decrease of the H–X stretching frequency and decrease of electron density of the H–X bond. The calculated values of electron density, $\rho(r)$, Laplacian of electron density, $\nabla^2\rho(r)$, and electronic energy density, H(r), at the bond and ring critical points (BCPs) at PBE1PBE/6-311++G(2d,2p) level of theory in the ground state are listed in Table 5. The AIM results for S_0–E, S_1–E and S_1–K states are given in Table S2 as a Supplementary data.

The electron density at H···N BCP gauges the strength of the intermolecular H-bond interaction, which are manifested by distance between H and N. Values of $\rho(r)$ at H···N BCP for **HBO** and **HNB1–3** are 0.0461, 0.0496, 0.0449 and 0.0624 au, respectively. Thus, H···N H-bonding in the **HNB3** is stronger than other molecules, in good agreement with the H-bond distance and H-bond energy calculated for **HNB3**. As can be seen, increase in $\rho(r)$ at O–H BCP is accompanied by a decrease in $\rho(r)$ at N···H BCP.

Nature of H-bond interactions involved in PT reaction can be more clearly understood from the $\nabla^2\rho(r)$ and H(r) values. The results in Table 5 show a positive value for $\nabla^2\rho(r)$ and a slightly negative value for H(r) at the N···H BCP. According to the Bader's criteria [48,49], nature of both OH···N and O···HN H-bonds are classified as partial covalency. The much more value of $\rho(r)$ (0.0624 au) together with the much more negative value of H(r) (−0.0155) at N···H BCP of **HNB3** with respect to those of other compounds implies that the covalency nature of the H-bonding in **HNB3** is greater than others, in good agreement with the much shorter H-bond distance found for **HNB3** than others. Accordingly, degree of covalency nature of N···H H-bonds is estimated as: **HNB3** > **HNB1** > **HBO** > **HNB2**.

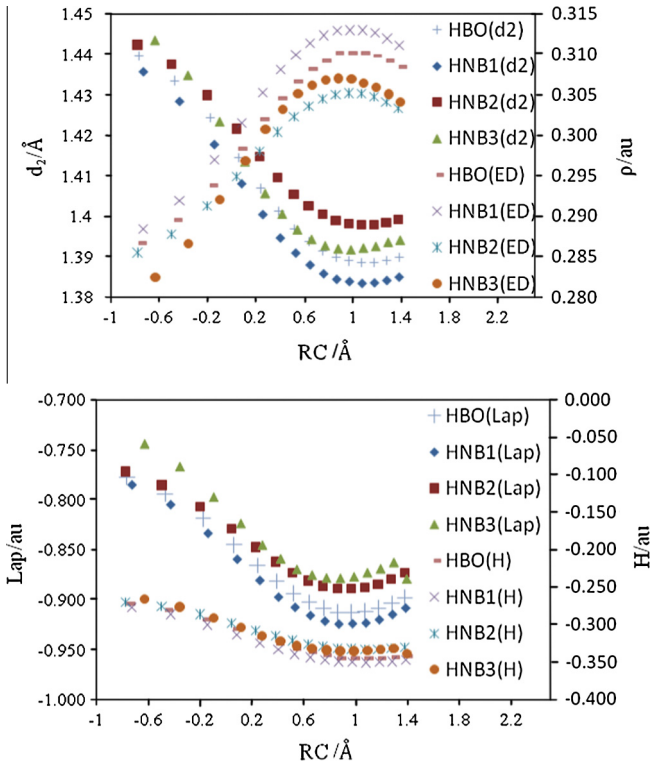

Fig. 7. Variation of electron density at the d2 BCP as well as d2 bond length versus RC (top) and Lapalcian of electron density (Lap) as well as electronic energy density (H) (bottom) along the PT pathway of the **HBO** and **HNB1–3** isomers at the S_0 state.

Fig. 6 shows the change in the $\rho(r)$ and $\nabla^2\rho(r)$ at the OH···N as well as O–HN bond critical points (BCPs) during the proton transfer reaction. As can be seen, increase in the $\rho(r)$ and $\nabla^2\rho(r)$ of OH···N bond is accompanied by decrease in those of the O–HN one. The similar results have been observed for 2-quinolin-2-yl-phenol [33,63].

The results reveal that the electron density at the N···H BCP increases upon photoexcitation to S_1–E state followed by a phototautomerization. In addition, covalency nature of OH···N increases upon photoexcitation from S_0–E to S_1–E.

The variation of C–C central bond (d2) and the corresponding electron density versus RC along the PT pathway of the **HBO** and **HNB1–3** isomers at the S_0 state is shown in Fig. 7 (top curve). As can be seen, d2 bond length decreases and electron density increases on going from E form to K one, indicating that the double nature of central C–C bond increases. The magnitude of decrease in electro density at d2 BCP is different for the studied molecules. Variation of Lapalcian of electron density as well as electronic energy density along the PT pathway of the **HBO** and **HNB1–3** isomers at the S_0 state is depicted in Fig. 7 (bottom curve). This figure illustrates that the negative value of Lapalcian of electron density as well as electronic energy density along the PT pathway increases.

The formation of the H-bonding in **HBO** and **HNB1–3** closes a 6-membered ring and is accompanied by the appearance of a ring critical point (RCP) in the proton transfer ring. The value of electron density at the RCP can provides the useful information regarding the ring electronic current and understanding the quality of the results. For E form of the **HBO** and **HNB1–3** molecules, value of electron density at the RCP of PT ring (ρ_{R1}) is smaller than that of the phenolic ring linked to PT ring (ρ_{R2}). Interestingly, values of ρ_{R1} and ρ_{R2} for the S_0–E forms are 0.0189 and 0.0237 au for **HBO**, 0.0197 au, 0.0230 au for **HNB1**, 0.0187 au and 0.0226 au for **HNB2** and 0.0210 au and 0.0223 au for **HNB3**, respectively. These values for S_1–E states are 0.0184 and 0.0225 au for **HBO,** 0.0208 and 0.0219 au for **HNB1**, 0.0227 au and 0.0219 au for **HNB2** and 0.0209 and 0.0212 au for **HNB3**, respectively. As can be seen, ρ_{R2} decreases upon photoexcitation from S_0–E to S_1–E. Besides, change in ρ_{R1} for **HNB2** is greater than others upon this photoexcitation.

Conclusions

Our studies demonstrate the relationship between the degree of π conjugation and the occurrence of ESIPT reaction. The results show that by modifying the resonance structure of **HBO**, a significant change on the physical and chemical properties is observed in the ground and excited electronic states. For all **HBO** and **HNB1–3**, the normal E forms were calculated to be the dominant ground state species. The instability of the K forms as well as high energy barrier for E to K transformation on discards any opportunity of the GSIPT process. But, access to S_1–K in the S_1 excited state is possible.

The absorption bands of **HNB1–3** in gas phase are red shifted with respect to those of **HBO**. Extension of the aromatic ring structure increases the energy gap between K forms of ground and excited states in the **HNB1** and **HNB3**. For **HNB2**, situation is opposite. It should be noted that the red shift observed in both absorption and emission bands of **HNB2** with respect to the **HBO** is remarkable. All three isomers and parent compound **HBO** exhibit Stokes-shifted fluorescence. The Stokes shift for **HNB2** in both gas phase and water is greater than others. It is also resulted that the emission spectrum of **HNB2** is more sensitive to solvent properties so that achieving a white light is much facilitated in solvents

with less polarity. The calculated fluorescence rate constant for phototautomeric (S_1–K) forms increases by raise in polarity of solvent and this increase for **HNB2** in both phases is smaller than other molecules. The results of population analysis show that the CT values at the S_0–E state increases on going from **HNB1** to the **HNB3**. In addition, redistribution of charge density in the **HNB2** upon phototatomerization is more significant than other molecules. The results of AIM analysis show that the electron density and covalency nature of the N···H BCP increases upon photoexcitation to S_1–E state.

Appendix A. Supplementary material

Supplementary data associated with this article can be found, in the online version, at http://dx.doi.org/10.1016/j.saa.2013.08.068.

References

[1] A.H. Weller, Prog. React. Kinet. 1 (1961) 187.
[2] R. Das, A.S. Klymchenko, G. Duportail, Y. Mely, J. Phys. Chem. B 112 (2008) 11929.
[3] A.S. Klymchenko, V.V. Shvadchak, D.A. Yushchenko, N. Jain, Y. Mely, J. Phys. Chem. B 112 (2008) 12050.
[4] C.L. Chen, C.W. Lin, C.C. Hsieh, C.H. Lai, G.H. Lee, C.C. Wang, P.T. Chou, J. Phys. Chem. A 113 (2009) 205.
[5] T. Mutai, H. Tomoda, T. Ohkawa, Y. Yabe, K. Araki, Angew. Chem., Int. Ed. 47 (2008) 9522.
[6] S.G. Roh, Y.H. Kim, K.D. Seo, D.H. Lee, H.K. Kim, Y.I. Park, J.W. Park, J.H. Lee, Adv. Funct. Mater. 19 (2009) 1663.
[7] A. Brenlla, F. Rodriguez-Prieto, M. Mosquera, M.A. Rios, M.C.R. Rodriguez, J. Phys. Chem. A 113 (2009) 56.
[8] J.M. Ortiz-Sanchez, R. Gelabert, M. Moreno, J.M. Lluch, J. Chem. Phys. 129 (2008) 214308.
[9] M. Gauden, A. Pezzella, L. Panzella, M.T. Neves-Petersen, E. Skovsen, S.B. Petersen, K.M. Mullen, A. Napolitano, M. Ischia, V. Sundstrom, J. Am. Chem. Soc. 130 (2008) 17038.
[10] W.H. Sun, S.Y. Li, R. Hu, Y. Qian, S.Q. Wang, G.Q. Yang, J. Phys. Chem. A 113 (2009) 5888.
[11] K.Y. Chen, Y.M. Cheng, C.H. Lai, C.C. Hsu, M.L. Ho, G.H. Lee, P.T. Chou, J. Am. Chem. Soc. 129 (2007) 4534.
[12] P.T. Chou, G.R. Wu, C.Y. Wei, M.Y. Shiao, Y.L. Liu, J. Phys. Chem. A 104 (2000) 8863.
[13] D. Kuila, G. Kvakovszky, M.A. Murphy, R. Vicari, M.H. Rood, K.A. Fritch, J.R. Fritch, S.T. Wellinghoff, S.F. Timmons, Chem. Mater. 11 (1999) 109.
[14] Z. Liang, Z. Liu, L. Jiang, Y. Gao, Tetrahedron Lett. 48 (2007) 1629.
[15] S.J. Lim, J. Seo, S.Y. Park, J. Am. Chem. Soc. 128 (2006) 14542.
[16] B.L. Feringa (Ed.), Molecular Switches, Wiley-VCH, Weinheim, Germany, 2001.
[17] Y. Wu, X. Peng, J. Fan, S. Gao, M. Tian, J. Zhao, S. Sun, J. Org. Chem. 72 (2007) 62.
[18] A. Sytnik, M. Kasha, Proc. Natl. Acad. Sci. U.S.A. 91 (1994) 8627.
[19] Y. Kubo, S. Maeda, S. Tokita, M. Kubo, Nature 382 (1996) 522.
[20] Q.J. Ma, X.B. Zhang, X.H. Zhao, Y.J. Gong, J. Tang, G.L. Shen, R.Q. Yu, Spectrochim. Acta Part A 73 (2009) 687.
[21] K.I. Sakai, M. Ichikawa, Y. Taniguchi, Chem. Phys. Lett. 420 (2006) 405.
[22] M. Zimmer, Chem. Rev. 102 (2002) 759.
[23] J. Catalan, J.C. Dell Valle, R.M. Claramunt, D. Saunz, J. Doctor, J. Lumin. 68 (1996) 165.
[24] L. Gagliardi, G. Orlandi, V. Molina, P.A. Malmqvist, B.O. Roos, J. Phys. Chem. A 106 (2002) 7355.
[25] J. Quenneville, T.J. Martinez, J. Phys. Chem. A 107 (2004) 829.
[26] Y. Dou, R.E. Allen, J. Chem. Phys. 119 (2003) 10658.
[27] D.M. Leitner, B. Levine, J. Quenneville, T.J. Martinez, P.G. Wolynes, J. Phys. Chem. A 107 (2003) 10706.
[28] R. Improta, F. Santoro, C. Dietl, E. Papastathopoulos, G. Gerber, Chem. Phys. Lett. 387 (2004) 509.
[29] C. Dietl, Papastathopoulos, P. Niklaus, R. Improta, F. Santoro, G. Gerber, Chem. Phys. 310 (2005) 201.
[30] R. Improta, F. Santoro, J. Phys. Chem. A 109 (2005) 10058.
[31] L. Biemann, S.A. Kovalenko, K. Kleinermanns, R. Mahrwald, M. Markert, R. Improta, J. Am. Chem. Soc. 133 (2011) 19664.
[32] H.G. Tsai, H.S. Sun, C. Tan, J. Phys. Chem. A 114 (2010) 4065.
[33] B.K. Paul, N. Guchhait, J. Lumin. 131 (2011) 1918.
[34] K. Sakota, C. Jouvet, C. Dedonder, M. Fujii, H. Sekiya, J. Phys. Chem. A 114 (2010) 11161.
[35] G. Cui, Z. Lan, W. Thiel, J. Am. Chem. Soc. 134 (2012) 1662.
[36] H. Gorner, H.J. Kuhn, Adv. Photochem. 19 (1995) 1.
[37] D. Panda, P.P. Mishra, S. Khatua, A.L. Koner, R.B. Sunoj, A. Datta, J. Phys. Chem. A 110 (2006) 5585.
[38] A. Szemik-Hojniak, I. Deperasinska, L. Jerzykiewicz, P. Sobota, M. Hojniak, A. Puszko, N. Haraszkiewicz, G. van der Zwan, P. Jacques, J. Phys. Chem. A 110 (2006) 10690.
[39] M. Higashi, S. Saito, J. Phys. Chem. Lett. 2 (2011) 2366.
[40] T. Iijima, A. Momotake, Y. Sinohara, T. Sato, J. Phys. Chem. A 114 (2010) 1603 (and references cited therein).
[41] S.R. Vazquez, M.C.R. Rodriguez, M. Mosquera, F. Rodriguez-Prieto, J. Phys. Chem. A 111 (2007) 1814.
[42] H. Wang, H. Zhang, O.K. Abou-Zied, C. Yu, F.E. Romesberg, M. Glasbeek, Chem. Phys. Lett. 367 (2003) 599.
[43] T. Arthen-Engeland, T. Bultmann, N.P. Ernsting, M.A. Rodriguez, W. Thiel, Chem. Phys. 163 (1992) 43.
[44] A. Fernandez-Ramos, J. Rodrıguez-Otero, M.A. Rios, J. Soto, J. Mol. Struct. (Theochem) 489 (1999) 255.
[45] C.R. Baiz, S.J. Ledford, K.J. Kubarych, B.D. Dunietz, J. Phys. Chem. A 113 (2009) 4862 (and references cited therein).
[46] H. Roohi, B. Moghadam, J. Mol. Model. 18 (2012) 1313.
[47] R.F.W. Bader, Atoms in Molecules. A Quantum Theory, Clarendon Press, Oxford, UK, 1990.
[48] R.F.W. Bader, H. Essen, J. Chem. Phys. 80 (1994) 1943.
[49] R.F.W. Bader, Can. J. Chem. 76 (1998) 973.
[50] C. Adamo, V. Barone, J. Chem. Phys. 110 (1999) 6158.
[51] C. Adamo, G.E. Scuseria, V. Barone, J. Chem. Phys. 111 (2000) 2889.
[52] M.J. Frisch, G.W. Trucks, H.B. Schlegel, G.E. Scuseria, M.A. Robb, J.R. Cheeseman, J.A. Montgomery, Jr., T. Vreven, K.N. Kudin, J.C. Burant, J.M. Millam, S.S. Iyengar, J. Tomasi, V. Barone, B. Mennucci, M. Cossi, G. Scalmani, N. Rega, G.A. Petersson, H. Nakatsuji, M. Hada, M. Ehara, K. Toyota, R. Fukuda, J. Hasegawa, M. Ishida, T. Nakajima, Y. Honda, O. Kitao, H. Nakai, M. Klene, X. Li, J.E. Knox, H.P. Hratchian, J.B. Cross, C. Adamo, J. Jaramillo, R. Gomperts, R.E. Stratmann, O. Yazyev, A.J. Austin, R. Cammi, C. Pomelli, J.W. Ochterski, P.Y. Ayala, K. Morokuma, G.A. Voth, P. Salvador, J.J. Dannenberg, V.G. Zakrzewski, S. Dapprich, A.D. Daniels, M.C. Strain, O. Farkas, D.K. Malick, A.D. Rabuck, K. Raghavachari, J.B. Foresman, J.V. Ortiz, Q. Cui, A.G. Baboul, S. Clifford, J. Cioslowski, B.B. Stefanov, G. Liu, A. Liashenko, P. Piskorz, I. Komaromi, R.L. Martin, D.J. Fox, T. Keith, M.A. Al-Laham, C.Y. Peng, A. Nanayakkara, M. Challacombe, P.M.W. Gill, B. Johnson, W. Chen, M.W. Wong, C. Gonzalez, J.A. Pople, Gaussian 03, Revision C.02, Gaussian, Inc., Wallingford CT, 2004.
[53] M. Cossi, N. Rega, M. Scalmani, V. Barone, J. Chem. Phys. 114 (2001) 5691.
[54] C.M. Breneman, K.B. Wiberg, J. Comp. Chem. 11 (1990) 361.
[55] F. Biegler-König, J. Schönbohm, D. Bayles, AIM2000-A program to analyze and visualize atoms in molecules, J. Comp. Chem. 22 (2001) 545.
[56] P. Gilli, V. Bertolasi, L. Pretto, L. Antonov, G. Gilli, J. Am. Chem. Soc. 127 (2005) 4943.
[57] K.-C. Tang, M.-J. Chang, T.-Y. Lin, H. -A Pan, T.-C. Fang, K.-Y. Chen, W.-Y. Hung, Y.-H. Hsu, P.-T. Chou, J. Am. Chem. Soc. 133 (2011) 17738.
[58] J.M. Hollas, Modern Spectroscopy, John Wiely & Sons Ltd., 1995.
[59] A.J.A. Aquino, H. Lischka, C. Hattig, J. Phys. Chem. A 109 (2005) 3201.
[60] A.E. Reed, L.A. Curtiss, F. Weinhold, Chem. Rev. 88 (1988) 899.
[61] U. Koch, P.L.A. Popelier, J. Phys. Chem. 99 (1995) 9747.
[62] P.L.A. Popelier, J. Phys. Chem. A 102 (1998) 1873.
[63] B.K. Paul, N. Guchhait, Comput. Theor. Chem. 978 (2011) 67.
[64] B.K. Paul, N. Guchhait, Comput. Theor. Chem. 966 (2011) 250.